Seasonality of submesoscale dynamics in the Kuroshio Extension

Cesar B. Rocha[1], Sarah T. Gille[1], Teresa K. Chereskin[1], and Dimitris Menemenlis[2]

Key Points.

- Upper-ocean submesoscale (10-100 km) turbulence and inertia-gravity waves undergo strong seasonal cycles that are out of phase.
- Submesoscale turbulence dominates the horizontal velocity and sea-surface height variability in late winter/early spring.
- Submesoscale inertia-gravity waves dominate the horizontal velocity and sea-surface height variability in late summer/early fall.

Two new high-resolution numerical simulations with embedded tides show a strong modulation of near-surface dynamics at submesoscales (roughly 10-100 km) in the Kuroshio Extension. Consistent with recent studies, deep late-winter mixed layers are prone to baroclinic instabilities, and submesoscale turbulence prevails in late winter/early spring. While summertime re-stratification weakens submesoscale turbulence, it also enhances submesoscale inertia-gravity waves near the surface. In the Kuroshio Extension, inertia-gravity waves strongly dominate the submesoscale surface kinetic energy and sea-surface height variance in late summer/early fall.

1. Introduction

Recent interest in upper-ocean dynamics has focused on the strong seasonal cycle of shallow baroclinic instabilities and their role in submesoscale (roughly 1-100 km) turbulence and mesoscale (roughly 100-300 km) modulation [*Sasaki et al.*, 2014; *Qiu et al.*, 2014; *Brannigan et al.*, 2015; *Callies et al.*, 2015; *Thompson et al.*, 2016; *Buckingham et al.*, 2016]. Contemporary studies have also shown that inertia-gravity waves (IGWs) contribute significantly to the near-surface variability at submesoscales [*Richman et al.*, 2012; *Bühler et al.*, 2014; *Rocha et al.*, 2016], but their seasonality has not been investigated.

Using the output of 1/24° and 1/48° global numerical simulations with embedded tides, we show that IGWs undergo a strong seasonality near the surface in the Kuroshio Extension region. Interestingly, the seasonal cycle of IGWs is out of phase with the seasonal cycle of submesoscale turbulence. On one hand, consistent with previous studies, deep late-winter mixed layers are prone to shallow baroclinic instabilities that are roughly in geostrophic balance and flux energy upscale [*Sasaki et al.*, 2014; *Callies et al.*, 2016], driving a mild seasonal modulation of the mesoscales [*Sasaki et al.*, 2014; *Qiu et al.*, 2014].

IGWs, on the other hand, peak in late summer/early fall, when the upper ocean is strongly stratified. Thus there exists a strong seasonal modulation of upper-ocean submesoscale dynamics: submesoscale turbulence dominates the upper-ocean dynamics in late winter/early fall, whereas submesoscale IGWs prevail in late summer/early fall. Because submesoscale turbulence is weakest in late summer/early fall, the present results indicate that IGWs account for most of the summertime submesoscale sea-surface height variability.

2. The LLC numerical simulations

We use results of two latitude-longitude polar cap (LLC) realistic numerical simulations. The outputs analyzed here, LLC2160 (1/24°) and LLC4320 (1/48°), are forward Massachusetts Institute of Technology general circulation model [MITgcm; *Marshall et al.*, 1997] numerical solutions on a LLC grid [*Forget et al.*, 2015] with 90-vertical-levels. The coarser-resolution LLC simulation was spun up from an Estimating the Circulation and Climate of the Ocean, Phase II [ECCO2; *Menemenlis et al.*, 2008] adjoint-method state estimate, constrained to millions of observations from 2009 through 2011. Both simulations were forced by tides hourly and by 6-hourly surface atmospheric fields. The LLC2160 output spans two years from March 2011 to April 2013; the LLC4320 was spun up from the LLC2160 simulation, spanning one year from September 2011 to October 2012. The LLC4320 simulation is an extension of the 3-month long output used by *Rocha et al.* [2016]. Details of the LLC simulations are provided in the supplemental material.

A key aspect of the LLC2160 and LLC4320 simulations is that they were forced by the 16 most-significant tidal components. Because barotropic tides interact with topography and generate internal tides that project onto mesoscales to submesoscales [e.g., *Rocha et al.*, 2016], tidal forcing fundamentally distinguishes our analysis from other modeling studies of seasonality [*Sasaki et al.*, 2014; *Qiu et al.*, 2014].

To study seasonal variations in the upper-ocean dynamics, we focus on the northwest Pacific, in the vicinity of the Kuroshio Extension, where previous studies have shown strong mesoscale and submesoscale seasonality [*Sasaki et al.*, 2014; *Qiu et al.*, 2014]. We analyze a sub-domain of the LLC4320 and LLC2160 simulations of about 2000 km^2 spanning 155-175°E; 25-40°N (Figure 1a). The stratification in this mesoscale-rich subtropical region undergoes a vigorous seasonal cycle: wintertime-enhanced small-scale turbulence de-stratifies the upper ocean, yielding mixed layers as deep as 300 m (Figure 1d). Summertime re-stratification yields mixed layers shallower than 40 m (Figure 1e). Fundamentally, the upper-ocean density structure is well-captured by both LLC simulations: a comparison with Argo climatology shows that both simulations skillfully represent the Kuroshio Extension stratification and its seasonal variability (supporting information).

[1]Scripps Institution of Oceanography, University of California San Diego, La Jolla, CA, USA.
[2]Earth Sciences Division, Jet Propulsion Laboratory, California Institute of Technology, Pasadena, CA, USA.

0094-8276/16/$5.00

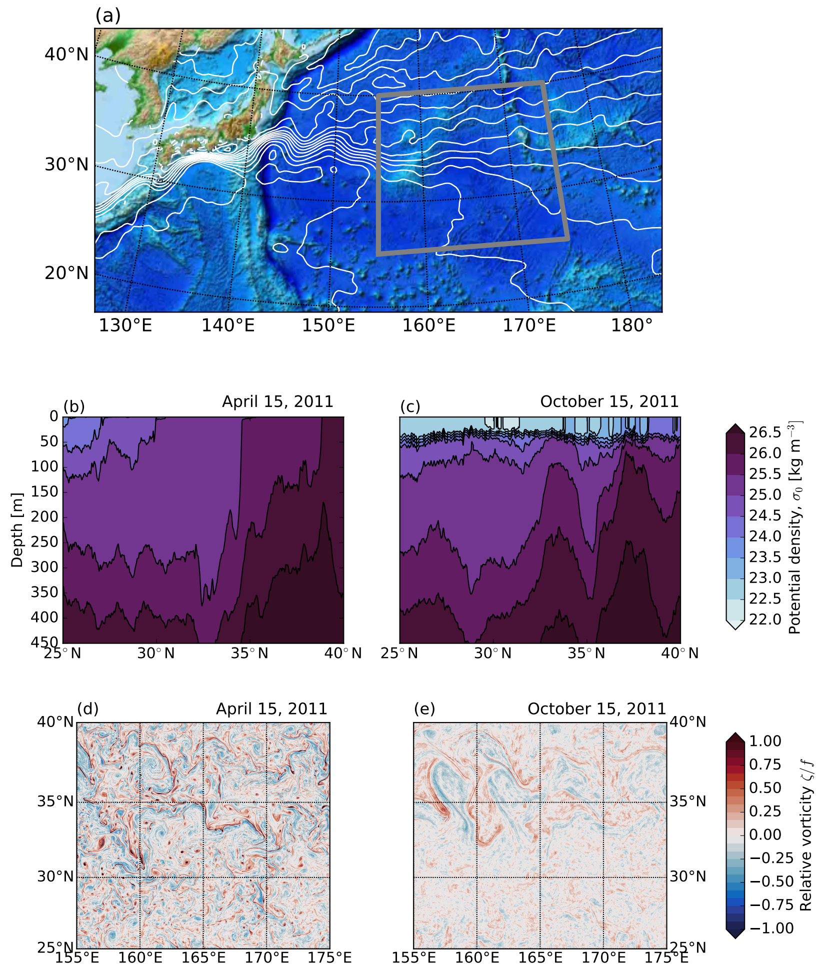

Figure 1. (a) The study region with the subregion where the LLC outputs are analyzed. Colors represent the topography and white lines are contours of absolute dynamic topography every 0.1 m from AVISO. LLC 4320 (1/48°) snapshots of transects of potential density at 165°E (b and c) and surface vorticity (d and e) . The snapshots were taken at 00:00 UTC.

3. Bulk statistics of the surface lateral velocity gradient tensor

To study the seasonality in the surface velocity, we calculate the lateral velocity gradient tensor

$$\begin{bmatrix} u_x & u_y \\ v_x & v_y \end{bmatrix} \tag{1}$$

using a centered second-order finite difference scheme. We then diagnose the vertical vorticity

$$\zeta \equiv v_x - u_y \,, \tag{2}$$

lateral rate of strain

$$\alpha \equiv \left[(u_x - v_y)^2 + (u_y + v_x)^2\right]^{1/2} , \tag{3}$$

and horizontal divergence

$$\delta \equiv u_x + v_y \,. \tag{4}$$

These diagnostics highlight the submesoscale structures in the flow [e.g., *Shcherbina et al.*, 2013].

Figures 1b-c show snapshots of vertical vorticity ζ in early spring (April 15) and fall (October 15) in the LLC4320 (1/48°) simulation. The model solutions depict seasonality in vorticity: large values of fine-grained vertical vorticity are observed in early spring with maximum values as large as $4f$, where f is the local planetary vorticity, and root-mean-square (RMS) of about $0.4f$. In early fall, the situation is the opposite: the vertical vorticity is relatively coarse-grained; its local maximum and RMS are both smaller than $0.5f$. Indeed, the vorticity and rate of strain are strongest in wintertime (Figure 2): in both simulations, the RMS vorticity and strain rate are about twice as large in late winter/early spring than in late summer/early fall. Because the wintertime vorticity and strain rate are dominated by the smallest scales in the flow (the KE spectrum is shallower than a -3 power law in winter), increasing the resolution from $1/24°$ to $1/48°$ increases the wintertime RMS vorticity and strain by about 40%.

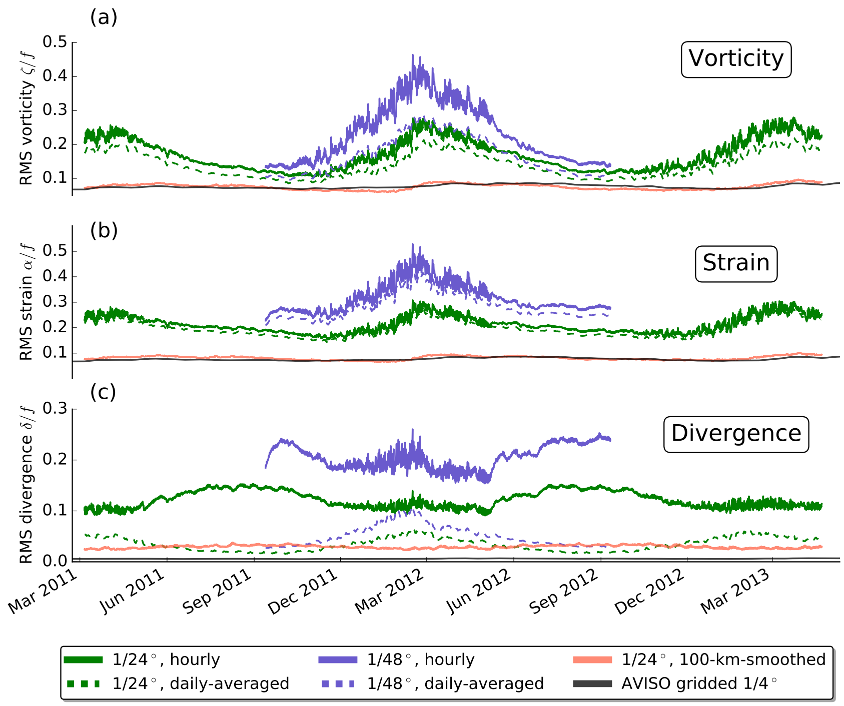

Figure 2. Time series of the root-mean-square (RMS) of surface (a) vorticity, (b) rate of strain, and (c) horizontal divergence in the LLC outputs and gridded AVISO data.

The bulk of vertical vorticity and strain rate are associated with subinertial flows ($T_f = 2\pi/f_0 \approx 23.5$h, where f_0 is the inertial frequency at the mean latitude): daily-averaging the velocity fields suppresses super-inertial motions and reduces the RMS vorticity by 40% and the RMS strain by 10%; the seasonal cycle remains strong (see dashed lines in figures 2a-b). Indeed, most of this seasonal cycle is associated with submesoscale flows: smoothing the velocity fields with a Hanning filter with cut off scale of 100 km dramatically reduces the RMS vorticity and strain rate. The reduction in variance is about 80% in winter, yielding RMS vorticity and strain rate roughly consistent with the diagnostics from AVISO gridded geostrophic velocities (compare red lines to black lines in figures 2a-b). The picture that emerges is consistent with recent studies: shallow baroclinic instabilities energize the submesoscales in winter, drawing from the available potential energy stored in large lateral buoyancy gradients in deep mixed layers [*Sasaki et al.*, 2014; *Callies et al.*, 2015, 2016].

The seasonal cycle of the horizontal divergence, however, showcases the complexity of the upper-ocean annual variability. If submesoscale eddies and fronts dominated the near-surface variability all year, then the seasonal cycle of horizontal divergence, vertical vorticity, and lateral strain rate would be in phase [e.g., *Sasaki et al.*, 2014]. While there is a clear wintertime peak in divergence of daily-averaged velocity (see dashed lines in figure 2c; RMS divergence $\sim 0.1f$ in the $1/48°$ simulation), the hourly fields show a stronger enhancement of lateral divergence in late summer/early fall (RMS divergence $\sim 0.22f$ the $1/48°$ simulation). Because the $1/48°$ simulation better resolves smaller-scale submesoscale flows, a secondary RMS divergence peak in winter is nearly as strong as in summer. Submesoscale fronts and eddies evolve relatively fast, and there is no clear temporal and spatial scale separation between those motions and IGWs [*McWilliams*, 2016]: daily-averaging the velocity fields efficiently suppresses the summertime horizontally divergent flows, but also reduces the wintertime lateral divergence by about 50%. Figure 2c also shows that most of the lateral divergence is associated with submesoscale flows: smoothing the velocity fields with a 100-km-cutoff suppresses more than 80% of the RMS divergence.

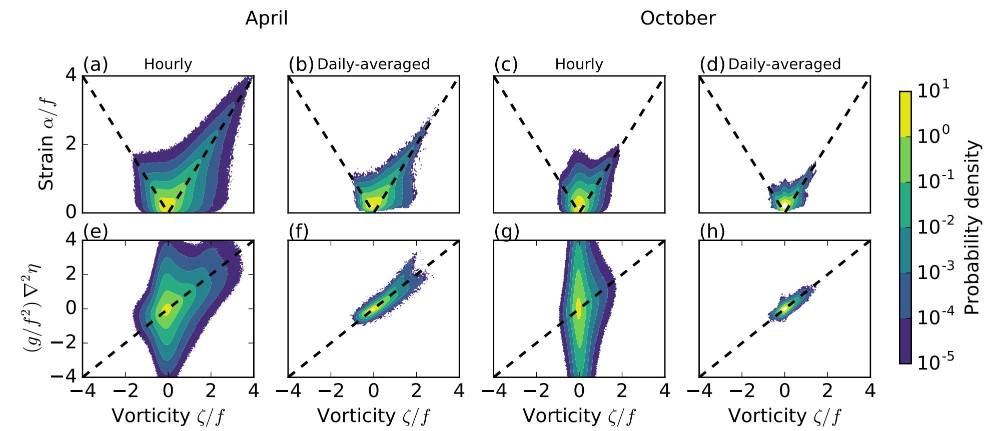

Figure 3. Seasonal variation of joint probability distributions of surface lateral velocity gradient tensor: vorticity vs. strain rate (a through d), and vorticity vs. Laplacian of sea-surface height (e through h) in April (a, b, e, f) and October (c, d, g, h). Dashed lines in (a) through (d) represent one dimensional shear flow $\alpha = \pm\zeta$, characteristic of fronts. Dashed lines in (e) through (h) represent geostrophic flow $\zeta = \frac{g}{f}\nabla_h^2\eta$.

4. Joint probability density functions

The results of figure 2a-c show that submesoscale surface variability stems from different dynamics in summer than in winter. To characterize these differences, we calculate joint probability distributions (joint-PDF) of vorticity-strain and vorticity-Laplacian of sea-surface height (Figure 3).

The April vorticity-strain joint-PDF has a shape characteristic of submesoscale turbulence (Figures 3a-b). The alignment of vorticity and strain $\alpha \sim \pm\zeta$ with strong positive skewness are fingerprints of submesoscale fronts [*Shcherbina et al.*, 2013; *McWilliams*, 2016]. The shape of the vorticity-strain joint-PDF is similar for hourly and daily-averaged fields, although the vorticity skewness reduces from 1.4 to 1.13 from hourly to daily-averaged. The April results are characteristic of winter, indicating that wintertime submesoscale surface velocity is strongly dominated by submesoscale turbulence. The hourly velocity and sea-surface heigh fields have an important ageostrophic component as depicted by the joint-PDF of vorticity-Laplacian of SSH winter (Figure 3e). In other words, even in April, when submesoscale turbulence prevails, only the daily-averaged fields are largely in geostrophic balance (the joint-PDF of daily-averaged vorticity vs.
Laplacian of sea-surface height is an ellipse with large eccentricity and main axis tilted by 45°; Figure 3f).

The October vorticity-strain joint-PDF shows much weaker skewness (the vorticity skewness is 0.68 and 0.67 for hourly and daily-averaged velocities). The shape of the vorticity-strain joint-PDF appears to be a combination of two half-ellipses centered about $\zeta = 0$, one with a 45° slope (characteristic of submesocale fronts that persist in summer) and one with a very steep slope. That the submesoscale dynamics in October are mainly ageostrophic is clearly depicted in the shape of joint-PDF of vorticity-Laplacian of sea-surface height for hourly fields (Figure 3g), which is an ellipse aligned in the vertical axis. Daily-averaging the model suppresses the ageostrophic, super-inertial flows, and, therefore, the daily-averaged flow is essentially geostrophic as depicted by the 45°-tilted ellipse in the vorticity-Laplacian of sea-surface height joint-PDF.

Time series of PDFs of vorticity and divergence (supporting information) show a strong oscillation between these two regimes. In late winter/early spring the vorticity is strongly positively skewed, whereas the divergence is moderately negatively skewed as predicted by frontogenesis [e.g., *McWilliams*, 2016] . In late summer/early fall, the divergence is stronger, but PDFs are much less skewed, consistent with linear IGWs.

5. Wavenumber-frequency spectrum

To confirm that inertia-gravity undergo a vigorous seasonal cycle near the surface, we calculate wavenumber-frequency spectrum of SSH variance. Focusing on the high-frequency content, we compute the wavenumber-frequency spectrum every 10 days and average the results to obtain a spectral estimate. Before calculating the each spectrum we remove linear trends and multiply the data by a three-dimensional Hanning window. The spectral estimate is then azimuthally-averaged in wavenumber.

Figures 4a-b show the wavenumber-frequency of SSH variance for the LLC4320 simulation. Mesoscales flows and the lunar semi-diurnal tide contain most of the SSH variance. But the is significant SSH variance at submesoscales, both subinertial and super-inertial. Subinertial SSH variance at submesoscales is larger in April, whereas super-inertial SSH variance at submesoscales is larger in October. Figure 4c, which shows the ratio between the two spectra, clearly depicts the out-of-phase seasonality of super-inertial and subinertial submesoscale flows. At scales smaller than 100 km (submesoscales), there the SSH variance is 66% larger in October than in April. More importantly, most of this SSH variance increase is accounted for IGWs, particularly modes two through four — higher vertical modes are more sensitive to changes in stratification (supporting information). Similarly, the submesoscale superinertial surface KE is 63% larger in October than the April.

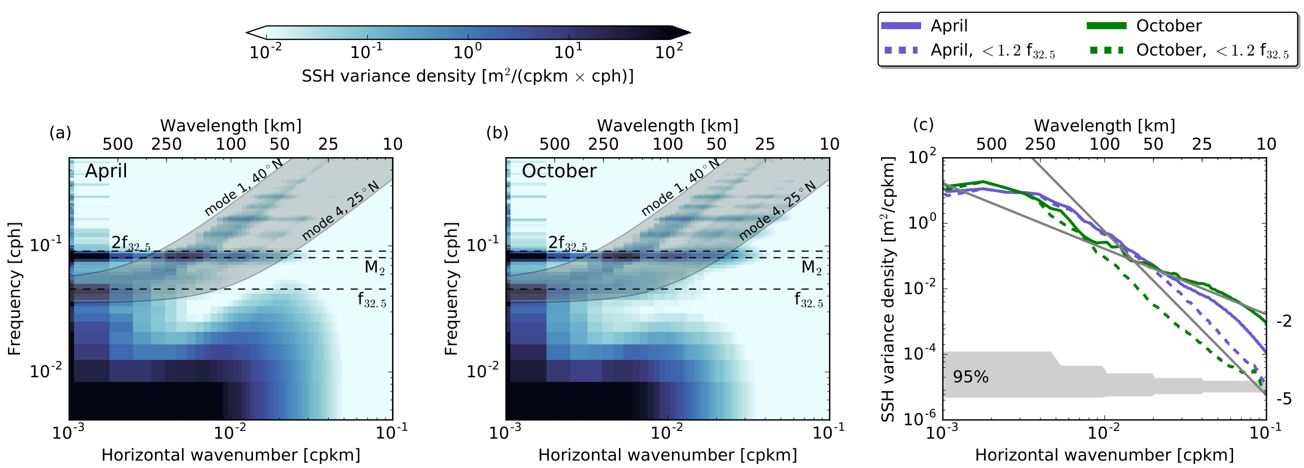

Figure 4. LLC4320 Wavenumber-frequency spectrum of SSH variance in (a) April and (b) October. (c) Wavenumber spectrum of SSH variance — the integral of (a) and (b) over frequency. In (a) and (b), the light gray shaded region depicts the dispersion relations for inertia-gravity waves from mode 1 through mode 4 across the latitudinal domain; horizontal dashed lines represent the semi-diurnal lunar tidal frequency (M_2), and the inertial frequency at mid-latitude ($f_{32.5}$) and its first harmonic ($2f_{32.5}$).

6. Discussion and conclusion

Our work adds to recent modeling [*Sasaki et al.*, 2014] and observational [*Callies et al.*, 2015; *Buckingham et al.*, 2016] evidence of vigorous seasonality in submesoscale turbulence. In particular, our main finding is that in global simulations with embedded tides the near-surface submesoscale IGWs in the Kuroshio Extension undergo a strong seasonal cycle that is out of phase with the seasonal cycle of submesoscale turbulence. We conjecture that the summertime dominance of IGWs [*Callies et al.*, 2015] is a consequence both of suppression of submesoscale turbulence and enhancement of IGWs due to re-stratification of the upper ocean.

D'Asaro [1978] showed that the velocity of linear internal waves in the mixed layer strongly depends on the density jump at the mixed layer base, with largest mixed layer velocities when the jump is strongest. In summer, the shallow mixed layer overlays a strong seasonal pycnocline, and thus the internal waves projection onto the mixed layer may be stronger according to *D'Asaro* [1978]'s arguments. An alternative explanation is that the shape of the baroclinic modes changes seasonally (supporting information).

Internal tide energy flux does not show a seasonal modulation [e.g., *Alford*, 2003], and therefore one expects a strong seasonality in the near-surface expression of internal tides and higher frequency IGWs generated through internal tide interactions. Windy near-inertial wave (NIW) generation is bursty and peaks in early winter, but NIW energy appears to have similar energy level in October and April [*Alford et al.*, 2016]. While NIWs are generated at large scales, mesoscale turbulence can refract and disperse those waves in few inertial periods, thereby generating submesoscale (10-100 km) near-inertial waves [*Alford et al.*, 2016]. But in our simulations the inertia-gravity-wave seasonality in submesoscale surface KE and SSH variance is mostly accounted for by higher frequency waves (Figure 4a-b), likely because submesoscale NIWs quickly propagate into the interior and have a small projection onto SSH.

An important caveat is that this study focuses on a single patch of ocean in the vicinity of the Kuroshio Extension. This may be typical of a mesoscale-rich subtropical region, but it is unlikely to be representative of other regions such as low-eddy-kinetic-energy eastern boundary currents and the middle of the subtropical gyre. We plan to report on the geographic variability of submesoscale seasonality in a future study.

Acknowledgments. William R. Young and the reviewers — Christian Buckingham and two anonymous referees — provided exceptionally helpful and constructive comments. Greg Wagner first suggested that the near-surface shape of the baroclinic modes may change seasonally. We thank the MITgcm community and our colleagues at the NASA Advanced Supercomputing (NAS) Division for their awesome support. This research was funded by NSF (OCE1357047) and NASA (NNX13AE44G,NNX13AE85G,NNX16AH67G). The LLC output can be obtained from the ECCO project (`http://ecco2.org/llc_hires`). The altimeter products were produced by Ssalto/Duacs and distributed by AVISO, with support from CNES (`http://www.aviso.altimetry.fr/duacs/`). Codes and output files are available online at the project repository (`https://github.com/crocha700/UpperOceanSeasonality`).

References

Alford, M. H. (2003), Redistribution of energy available for ocean mixing by long-range propagation of internal wave, *Nature*, *423*(6936), 159–162.

Alford, M. H., J. A. MacKinnon, H. L. Simmons, and J. D. Nash (2016), Near-inertial internal gravity waves in the ocean, *Annual review of marine science*, *8*, 95–123.

Brannigan, L., D. P. Marshall, A. Naveira-Garabato, and A. G. Nurser (2015), The seasonal cycle of submesoscale flows, *Ocean Modelling*, *92*, 69–84.

Buckingham, C. E., A. C. Naveira Garabato, A. F. Thompson, L. Brannigan, A. Lazar, D. P. Marshall, A. George Nurser, G. Damerell, K. J. Heywood, and S. E. Belcher (2016), Seasonality of submesoscale flows in the ocean surface boundary layer, *Geophysical Research Letters*, *43*(5), 2118–2126.

Bühler, O., J. Callies, and R. Ferrari (2014), Wave–vortex decomposition of one-dimensional ship-track data, *Journal of Fluid Mechanics*, *756*, 1007–1026.

Callies, J., R. Ferrari, J. M. Klymak, and J. Gula (2015), Seasonality in submesoscale turbulence, *Nature communications*, *6*.

Callies, J., G. Flierl, R. Ferrari, and B. Fox-Kemper (2016), The role of mixed-layer instabilities in submesoscale turbulence, *Journal of Fluid Mechanics*, *788*, 5–41.

D'Asaro, E. A. (1978), Mixed layer velocities induced by internal wave, *Journal of Geophysical Research: Oceans*, *83*(C5), 2437–2438.

Forget, G., J.-M. Campin, P. Heimbach, C. Hill, R. Ponte, and C. Wunsch (2015), ECCO version 4: an integrated framework for non-linear inverse modeling and global ocean state estimation, *Geosci. Model Dev.*, *8*, 3071–3104.

Marshall, J., C. Hill, L. Perelman, and A. Adcroft (1997), Hydrostatic, quasi-hydrostatic, and nonhydrostatic ocean modeling, *Journal of Geophysical Research: Oceans*, *102*(C3), 5733–5752.

McWilliams, J. C. (2016), Submesoscale currents in the ocean, in *Proc. R. Soc. A*, vol. 472, p. 20160117, The Royal Society.

Menemenlis, D., J.-M. Campin, P. Heimbach, C. Hill, T. Lee, A. Nguyen, M. Schodlok, and H. Zhang (2008), ECCO2: High resolution global ocean and sea ice data synthesis, *Mercator Ocean Quarterly Newsletter*, *31*, 13–21.

Qiu, B., S. Chen, P. Klein, H. Sasaki, and Y. Sasai (2014), Seasonal mesoscale and submesoscale eddy variability along the North Pacific Subtropical Countercurrent, *Journal of Physical Oceanography*, *44*(12), 3079–3098.

Richman, J. G., B. K. Arbic, J. F. Shriver, E. J. Metzger, and A. J. Wallcraft (2012), Inferring dynamics from the wavenumber spectra of an eddying global ocean model with embedded tides, *Journal of Geophysical Research: Oceans*, *117*(C12).

Rocha, C. B., T. K. Chereskin, S. T. Gille, and D. Menemenlis (2016), Mesoscale to submesoscale wavenumber spectra in Drake Passage, *Journal of Physical Oceanography*, *46*, 601–620.

Sasaki, H., P. Klein, B. Qiu, and Y. Sasai (2014), Impact of oceanic-scale interactions on the seasonal modulation of ocean dynamics by the atmosphere, *Nature communications*, *5*.

Shcherbina, A. Y., E. A. D'Asaro, C. M. Lee, J. M. Klymak, M. J. Molemaker, and J. C. McWilliams (2013), Statistics of vertical vorticity, divergence, and strain in a developed submesoscale turbulence field, *Geophysical Research Letters*, *40*(17), 4706–4711.

Thompson, A. F., A. Lazar, C. Buckingham, A. C. Naveira Garabato, G. M. Damerell, and K. J. Heywood (2016), Open-ocean submesoscale motions: A full seasonal cycle of mixed layer instabilities from gliders, *Journal of Physical Oceanography*, *46*(4), 1285–1307.

Corresponding author: Cesar B. Rocha, Scripps Institution of Oceanography, University of California San Diego, La Jolla, CA, USA. (crocha@ucsd.edu)